The effect of field-aligned currents and centrifugal forces on ionospheric outflow at Saturn

C. J. Martin[1], L. C. Ray[1], M. Felici[2], D. A. Constable[1], C. T. S. Lorch[1], J. Kinrade[1], R. L. Gray[3]

[1]Department of Physics, Lancaster University, Bailrigg, Lancaster, U.K., LA1 4YB
[2]Centre for Space Physics, Boston University, Boston, MA, USA
[3]Department of Engineering, Lancaster University, Bailrigg, Lancaster, U.K., LA1 4YW

Key Points:

- An ionospheric outflow model is developed for use at Saturn's auroral regions
- The presence of field-aligned currents and centrifugal forces enhances outflow by an order of magnitude
- Predicted total outflow flux rate of $5.5 - 13.0 \times 10^{27}\,\mathrm{s}^{-1}$ is comparable to flux calculated from Cassini data

Corresponding author: C. J. Martin, `c.martin1@lancaster.ac.uk`

Abstract

Ionospheric outflow is driven by an ambipolar electric field induced due to the separation of electrons and ions in a gravitational field when equilibrium along a magnetic field line is lost. A model of ionospheric outflow at Saturn was developed using transport equations to estimate the number of charged particles that flow from the auroral regions into the magnetosphere. The model evaluates the outflow from 1400 km in altitude above the 1 bar level, to 3 R_S along the field line. The main ion constituents evaluated are H^+ and H_3^+. We consider the centrifugal force exerted on the particles due to a fast rotation rate, along with the effects of field-aligned currents present in the auroral regions. The total number flux from both auroral regions is found to be $5.5 - 13.0 \times 10^{27}\,s^{-1}$, which relates to a total mass source of 5.5-17.7 $kg\,s^{-1}$. These values are on average an order of magnitude higher than expected without the additional effects of centrifugal force and field-aligned currents. We find the ionospheric outflow rate to be comparable to the lower estimates of the mass-loading rate from Enceladus and are in agreement with recent Cassini observations. This additional mass flux into the magnetosphere can substantially affect the dynamics and composition of the inner and middle magnetosphere of Saturn.

1 Introduction

Axford (1968) first theorised that the polar wind is a supersonic flow of charged particles from the ionosphere along open field lines at Earth. The polar wind at Earth is caused by an ambipolar electric field arising from the separation of ions and electrons due to gravity. This electric field accelerates the ions outward along the field lines to maintain quasi-neutrality. Hoffman (1970) used Explorer 31 satellite data to first observe H^+ outflow at Earth. Earth's polar wind is dominated by H^+ and O^+ ions, the lightest and dominant ionospheric constituents, respectively. The reader is directed to Yau et al. (2007) for an extensive review of polar wind observations at Earth.

However, to initiate this process, a mechanism is required to de-stablise the equilibrium along a field line and at Earth this is the Dungey cycle (Dungey, 1961). Plasma along a field line on the dayside of the magnetosphere is in equilibrium until the field line reconnects with the solar wind. The solar wind end of the field line has a much lower density and pressure, resulting in a pressure gradient along the field line. As the field line convects over the polar cap, the plasma moves along it until it sinks into the tail and reconnects once again. Any plasma remaining planet-ward of the reconnection x-line will then be trapped inside the magnetosphere, and hence will populate the magnetosphere with ionospheric plasma (Yamauchi, 2019).

At Saturn, the ionospheric outflow is expected to be composed of H^+ and H_3^+. Furthermore, only a small area of the very high latitude ionosphere and a slice of the magnetosphere in the dayside and dawn flanks are expected to be susceptible to large-scale reconnection (Desroche et al., 2013; Masters et al., 2012) and thus contain a Dungey-style plasma convection cycle (Cowley et al., 2003). The Dungey cycle at Saturn has been estimated to take around one week to flow through a whole cycle (Jackman et al., 2004). If the polar wind travels at $\sim$10 kms^{-1}, for example, the Dungey reconnection x-line would need to be at over 65 R_S (1 R_S = 60,268 km) for $\sim$57% of the plasma to be retained by the magnetosphere (Glocer et al., 2007). Felici et al. (2016) observed outflow of H^+ at 36 R_S using the CAPS instrument on board the Cassini spacecraft, on field lines connected to the ionosphere in the tail of the magnetosphere. From this measurement of outflow, a total particle flux of $(6.1\pm2.9)\times10^{27}\,s^{-1}$ and $(2.9\pm1.4)\times10^{28}\,s^{-1}$ can be calculated. This number flux relates to a mass flux of 10 ± 4 and $49 \pm 23\,kg\,s^{-1}$.

Saturn's magnetosphere is predominantly rotationally driven (Southwood & Kivelson, 2001) with internal plasma sources, such as the moon Enceladus. Enceladus releases $\sim 10^{27} - 10^{28}$ water molecules per second into the magnetosphere of Saturn (e.g., Jurac et al., 2002; Jurac & Richardson, 2005, 2007), which are then ionised to form a plasma torus around Saturn at Enceladus' orbit at $4\,R_S$. The plasma around Enceladus is bound to the magnetic field, mass-loading the system, and is swept up in the corotational flow around the planet. The stress due to mass loading drives an enforcement current system coupled to the ionosphere (Pontius & Hill, 1982; Pontius, 1995). Pontius and Hill (2006) show that to produce the perturbations in velocity of ions due to this current system, there must be at least 100 kg of matter being ionised at Enceladus every second. Additionally, model estimates from Fleshman et al. (2013) place the mass production rate of plasma at Enceladus at 60-100 $kg\,s^{-1}$. As such Enceladus is considered the dominant plasma source in Saturn's magnetosphere.

An additional source of plasma in Saturn's magnetosphere is the solar wind. The solar wind interaction is partly driven by possible viscous interactions at the magnetopause boundary (e.g., Delamere & Bagenal, 2010; Desroche et al., 2013). The total mass source of the solar wind can be estimated using the solar wind mass flux (Hill, 1979; Hill et al., 1983; Vasyliūnas, 2008; Bagenal & Delamere, 2011). Felici et al. (2016) estimated a number flux source of 8.21×10^{27} - $2.46\times10^{30}\,s^{-1}$. Assuming that hydrogen H^+ is the dominant constituent of the solar wind this corresponds to a source rate of 0.013-4.119 $kg\,s^{-1}$. As such we can consider the solar wind, to be a minor contributing source of magnetospheric plasma at Saturn, affecting mostly the outer magnetosphere, compared to the inner and middle where the ionospheric outflow is present.

The relative abundances of water group ions (sourced from Enceladus) and less massive hydrogen-based ions (sourced from the ionosphere or solar wind) is an important factor in controlling the dynamics of Saturn's magnetosphere. However, due to the difference in source mechanisms at the giant planets, we hereafter refer to the outflow of plasma as ionospheric outflow. The importance of the ionospheric outflow as a source of plasma at Saturn has previously been assessed by Glocer et al. (2007) using a hydrodynamic, multi-fluid model based on the polar wind model developed earlier at Earth by Gombosi et al. (1985). Glocer et al. (2007) find a particle source rate of 2.1×10^{26} - $7.5\times10^{27}\,s^{-1}$, an order of magnitude lower than that found by Felici et al. (2016). This difference may be due to the event described in Felici et al. (2016) having occurred during a time of high solar wind dynamic pressure, compressing the magnetosphere. Additionally, centrifugal forces (CFs) and the effects of field-aligned currents (FACs) on ionospheric outflow rates were not considered by Glocer et al. (2007).

The following section outlines the multi-fluid model used in this study, previously developed for the Jupiter system by Martin et al. (Submitted). This ionospheric outflow model accounts for the CF acting on the plasma due to the quick rotation of Saturn's magnetosphere, plus the presence of FACs in the auroral regions. We then present the outputs of the model with and without FACs and CF, by running the model to quasi-steady state over a range of initial conditions. We conclude with a discussion of the implications of the different mass sources and compare the rates at which they populate Saturn's magnetosphere.

2 Model

The model of ionospheric outflow described here is a hydrodynamic, 1-D, multi-fluid model that evaluates one flux tube with an expanding cross-section of A, where the spatial domain is along the field line. The flux tube cross-section increases with the reciprocal of the magnetic field strength which, out to a distance of 3 R_S, we assume to be a dipole. The model evaluates two ion species, H^+ and H_3^+, using the five-moment gyrotropic transport equations (Banks & Kockarts, 1973). These are the continuity of mass (equation 1), continuity of momentum (equation 2) and continuity of energy (equation 3) in a closed system which include contributions from CFs, pressure gradients, gravitational forces and the ambipolar electric field.

$$\frac{\partial}{\partial t}(A\rho_i) = -\frac{\partial}{\partial r}(A\rho_i u_i) + AS_i \tag{1}$$

$$\frac{\partial}{\partial t}(A\rho_i u_i) = -\frac{\partial}{\partial r}(A\rho_i u_i^2) - A\frac{\partial P_i}{\partial r} + A\rho_i\left(\frac{e}{m_i}E_\parallel - g + \omega^2 r\right) + \frac{\delta M_i}{\delta t} + Au_iS_i \tag{2}$$

$$\frac{\partial}{\partial t}(\frac{1}{2}A\rho_i u_i^2 + AP_i\frac{1}{\gamma_i - 1}) = -\frac{\partial}{\partial r}(\frac{1}{2}A\rho_i u_i^3 - Au_iP_i\frac{\gamma_i}{\gamma_i - 1}) + Au_i\rho_i\left(\frac{e}{m_i}E_\parallel - g + \omega^2 r\right) + \frac{\partial}{\partial r}\left(A\kappa_i\frac{\partial T_i}{\partial r}\right) + \frac{\delta M_i}{\delta t} + \frac{\delta E_i}{\delta t} + \frac{1}{2}Au_i^2S_i \tag{3}$$

Equations 2 and 3 evaluate the acceleration due to the electric field ($\frac{e}{m_i}E_\parallel$), the acceleration due to gravity (g) and the centrifugal acceleration term ($\omega^2 r$), where ω is angular velocity due to corotation and r is distance along a field line. All these terms are evaluated along the field line by calculating the field-aligned component of the acceleration. Subscript 'i' denotes the ionic species, A is the flux tube cross section described earlier, ρ is mass density, u is velocity, S is the mass production rate, P is pressure, e is electron charge, m is the mass of the ion species, g is gravitational acceleration, κ is the thermal conductivity, T is temperature and γ is the specific heat ratio.

$\frac{\partial}{\partial r}\left(A\kappa_i\frac{\partial T_i}{\partial r}\right)$ is considered negligible (magnitude is < 0.5% compared to the largest term in equation 3) in this formulation. This is determined by magnitude analysis at the first iterations, for this purpose only, κ is included in the initial conditions. When the term is small it is removed to improve computational efficiency. For ions, $\kappa_i = 4.6 \times 10^6 \frac{m_i}{m_p}^{-0.5} T^{5/2} e\,\mathrm{Jm^{-1}s^{-1}K^{-1}}$ and for electrons $\kappa_e = 1.8 \times 10^8 T^{5/2} e\,\mathrm{Jm^{-1}s^{-1}K^{-1}}$ (Banks & Kockarts, 1973), where m_p is the proton mass and m_i is the ion mass.

The parallel electric field ($E_\parallel$) produced by the net charge separation is given by:

$$E_\parallel = -\frac{1}{en_e}\left(\frac{\partial}{\partial r}(P_e - \rho_e u_e^2) + \frac{\frac{dA}{dr}}{A}\rho_e u_e^2\right) + \frac{1}{en_e}\frac{\partial}{\partial r}\left(\sum_i \frac{m_e}{m_i}\left((u_e - u_i)S_i - \frac{\delta M_i}{\delta t}\right) + \frac{\delta M_e}{\delta t}\right) \tag{4}$$

Subscript 'e' denotes the quantity for an electron and n is the number density. $\frac{\delta M_i}{\delta t}$ (momentum exchange rate) and $\frac{\delta E_i}{\delta t}$ (energy exchange rate) are given by:

$$\frac{\delta M_i}{\delta t} = -\sum_y \rho_i \nu_{iy}(u_i - u_y) \tag{5}$$

$$\frac{\delta E_i}{\delta t} = \sum_y \frac{\rho_i \nu_{iy}}{m_i + m_y}\left(3k_b(T_y - T_i) + m_y(u_i - u_y)^2\right) \tag{6}$$

Subscript 'y' denotes a neutral species, which in this model are H_2, He, H and H_2O. ν_{iy} is the collision frequency between the ionic species and neutral species (equation 7), where λ_y is the neutral gas polarisability which are $0.82 \times 10^{-30}\,\mathrm{m^3}$, $0.21 \times 10^{-30}\,\mathrm{m^3}$, $0.67 \times 10^{-30}\,\mathrm{m^3}$ and $1.48 \times 10^{-30}\,\mathrm{m^3}$ for H_2, He, H and H_2O respectively (Schunk & Nagy, 2000). k_b is the Boltzmann constant. We assume the neutral atmosphere is at rest (u_y =0). The momentum exchange rate for electrons $\frac{\delta M_e}{\delta t}$ is considered negligible compared to the dominant electron pressure gradient in equation 4.

$$\nu_{iy} = 2.21\pi\frac{\rho_y}{m_i + m_y}\sqrt{\frac{\lambda_y e^2}{\frac{m_i m_y}{m_i + m_y}}} \tag{7}$$

We use charge neutrality (8) and a steady state electron velocity assumption (9) to solve for the density and velocity of the electrons. To solve the energy of the electrons we use an electron energy equation (10).

$$n_e = \sum_i n_i \tag{8}$$

$$u_e = \frac{1}{n_e}\left(\sum_i n_i u_i - \frac{j}{e}\right) \tag{9}$$

$$\begin{aligned}\rho_e \frac{\partial T_e}{\partial t} &= -\rho_e u_e \frac{\partial T_e}{\partial r} - T_e\left(S_e + \frac{\gamma_e - 1}{A}\rho_e \frac{\partial}{\partial r}(Au_e)\right) \\ &+(\gamma_e - 1)\frac{m_e}{k_b}\frac{\delta E_e}{\delta t} + (\gamma_e - 1)\frac{m_e}{k_b A}\frac{\partial}{\partial r}\left(A\kappa_e \frac{\partial T_e}{\partial r}\right)\end{aligned} \tag{10}$$

$\frac{\delta E_e}{\delta t}$ and $\frac{\partial}{\partial r}\left(A\kappa_e \frac{\partial T_e}{\partial r}\right)$ are negligible. j is the current density of FACs which is scaled using the flux tube cross-section, $j = j_0 A_0/A$, where j_0 is the current density at a reference altitude A_0. The value of j_0 used is from a range between 55 - 572 nA m^{-2} (Ray et al., 2013) at a height of 1000 km, or roughly the peak in ionospheric electron density.

The model has a temporal resolution of 0.01 s. The field line is split into a spatial grid of 75 km-wide cells. This relates to 2400 grid cells for a field line of length 3.0 R_S. The spatial derivatives used in the above equations are estimated using central difference Euler for first order derivatives, and forward Euler for temporal derivatives. This method is used because the terms are not stiff (or become unstable) when using a time step of 0.01 s or less. Results are robust when using spatial grid sizes from 20-75 km, so for computational efficiency we use 75 km.

The initial parameters are the temperature and density distributions along the field line which are found using Moore et al. (2008) for ions and Banks and Kockarts (1973) & Schunk and Nagy (2000) for neutrals. All other variables are derived using the following formulations: velocity is found from equating the thermal energy to the kinetic energy, $u_i = \sqrt{\frac{2k_bT_i}{m_i}}$; mass production rate is estimated as a 1% fraction of the mass density (results are robust against a 2 order of magnitude change in this value, and are comparable to reaction rates derived by (Moses & Bass, 2000)); and pressure is calculated from the plasma pressure equation, $P_i = n_i k_b T_i$.

Initial values of density for the ionic and neutral species are extrapolated with an exponential decay, with appropriate scale height, from 1400 km to a minimum background value (to avoid a perfect vacuum). Initial values can be found in figure 1, along with the flux tube cross-sectional area. The model is run until quasi-steady-state is reached, or until the difference between two iterations is less than 0.1%. The electron flux along a flux tube is calculated as the product of the electron number density and electron velocity ($n_e u_e$), multiplied by A, the cross-sectional area of the flux tube.

3 Results

Figure 2 shows result from an auroral atmosphere which includes FACs and CF. From top to bottom are the parallel electric field in panel a, acceleration due to gravity (dash-dotted teal), CF (dashed purple) and the electric fields acting on H^+ (dark blue) and H_3^+ (light blue) in panel b. Individual ion fluxes can also be calculated for each species shown in panel c and the electron flux in panel d. The FAC in this example is 500 nA m^{-2}, an upper value of the range given by Ray et al. (2013). Gravitational acceleration dominates between 0.7 R_S and 1.5 R_S, with centrifugal acceleration dominating outside. The

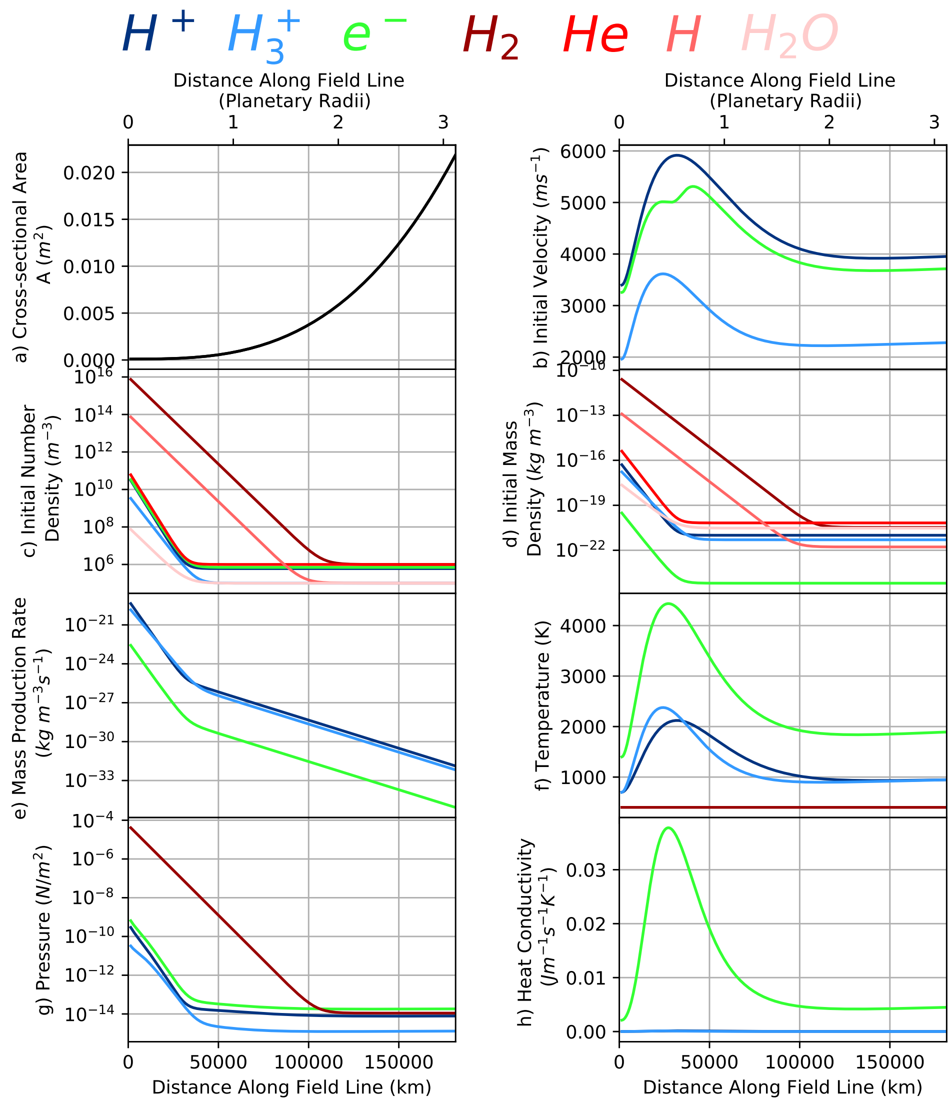

Figure 1. Initial conditions: a) cross-sectional area of flux rope, b) velocity of ions and electrons (neutral velocity is 0 kms^{-1}), c) number density of ions, electrons and neutrals, d) mass density of ions, electrons and neutrals, e) mass production rate of ions and electrons, f) temperature profile of ions, electrons and neutrals (neutrals all have the same temperature), g) pressure of ions, electrons and neutrals (only total neutral pressure shown) and h) thermal conductivity of ions and electrons, for the ionospheric outflow model along a field line from 1400 km to 3.0 R_S from the 1 bar level. Ions are shown in blue, electrons in green and neutrals in red. The key to the different colours is at the top of the figure.

Table 1. Comparison of five model runs over an area of specified 'oval size' in degrees wide to show the large variation in particle and mass source rates. Run 1 includes field-aligned currents and centrifugal forces for average initial conditions presented in Figure 2. Run 2 does not include field-aligned currents and centrifugal forces for average initial conditions presented in figure 3. Run 3 shows an example of a run for the sub-auroral regions. Runs 4 and 5 show the two extremes of initial conditions from which we calculate the range of total particle and mass source rates including field-aligned currents and centrifugal force.

Input Variables	Run 1 Auroral	Run 2 Terrestrial-like	Run 3 Sub-Auroral	Run 4 Min	Run 5 Max
n_{H^+} [m^{-3}]	5×10^{10}	5×10^{10}	5×10^{10}	5×10^{9}	2×10^{11}
$n_{H_3^+}$ [m^{-3}]	2×10^{10}	2×10^{10}	2×10^{10}	7×10^{8}	1×10^{11}
$T\,[K]$	700	700	700	200	2000
j (peak value) $[n\mathrm{A}m^{-2}]$	500	0	0	50	500
Oval size (°)	2	2	10	2	2
Output Variables					
Total particle source rate $[s^{-1}]$	1.0×10^{28}	3.9×10^{27}	1.3×10^{28}	5.5×10^{27}	1.3×10^{28}
Total mass source rate [kg s^{-1}]	13.1	3.2	17.7	5.5	17.7

electric field peaks within 0.5 $\mathrm{R_S}$ and reduces with distance along the field line. By 1 $\mathrm{R_S}$ along the field line, both the ion and electron fluxes reduce to a steady value with distance.

An auroral oval of approximately 2° latitudinal width centered at 14° colatitude is assumed, multiplying the number flux along each field line within the auroral oval, where we have a 1° upward current and 1°-wide downward current of 1/3 of the strength of the upward current is used. This is summated around the entire polar cap and multiplied by 2 (for both hemispheres) to return a total particle source rate for the entire auroral regions, excluding the high latitude polar cap. The initial conditions in figure 1 including the FACs and CFs give a total particle source rate of $1.0{\times}10^{28}\,\mathrm{s}^{-1}$. Taking into consideration the relative flux rates of the electrons and ions, this gives a total mass source rate of 13.1 kg s^{-1}.

We note, however, that the initial conditions are the same for Runs 1 and 2 for the entire polar cap. The temperature and density of the electrons and ions, though, will vary significantly within this area. The FAC strengths also vary on a order of magnitude (Ray et al., 2013). As such, to determine an uncertainty in the output of the model, we vary n_{H^+} between 5×10^9 and $2 \times 10^{11}\,\mathrm{m}^{-3}$, $n_{H_3^+}$ between 7×10^9 and $1 \times 10^{11}\,\mathrm{m}^{-3}$ as well as varying the temperature between 200 - 2000 K. The FACs are varied between 50-500 nAm^{-2} (Ray et al., 2013). Hence, we find a range of total particle source rates, from $5.5{\times}10^{27}$ to $1.3 \times 10^{28}\,\mathrm{s}^{-1}$ corresponding to a total mass source rate of $5.5 - 17.7\,\mathrm{kg\,s}^{-1}$.

Figure 3 (run 2) shows the results for the same initial conditions as figure 2, however this run removed the FACs and CFs (shown as a constant value of 0 in the figure). The electric field is similar in shape to Figure 2 but is reduced in magnitude. By 1 $\mathrm{R_S}$ along the field line again, both the ion and electron fluxes reduce to a steady value with distance. Using the same formulation as above, the range of total particle source rates from a 2° auroral oval is $8.9{\times}10^{26}$ to $6.8{\times}10^{27}\,\mathrm{s}^{-1}$ corresponding to a total mass source of $0.9 - 6.8\,\mathrm{kg\,s}^{-1}$, which is an order of magnitude lower than the results from the inclusion of CFs and FACs. The ranges of the input values (number density and temper-

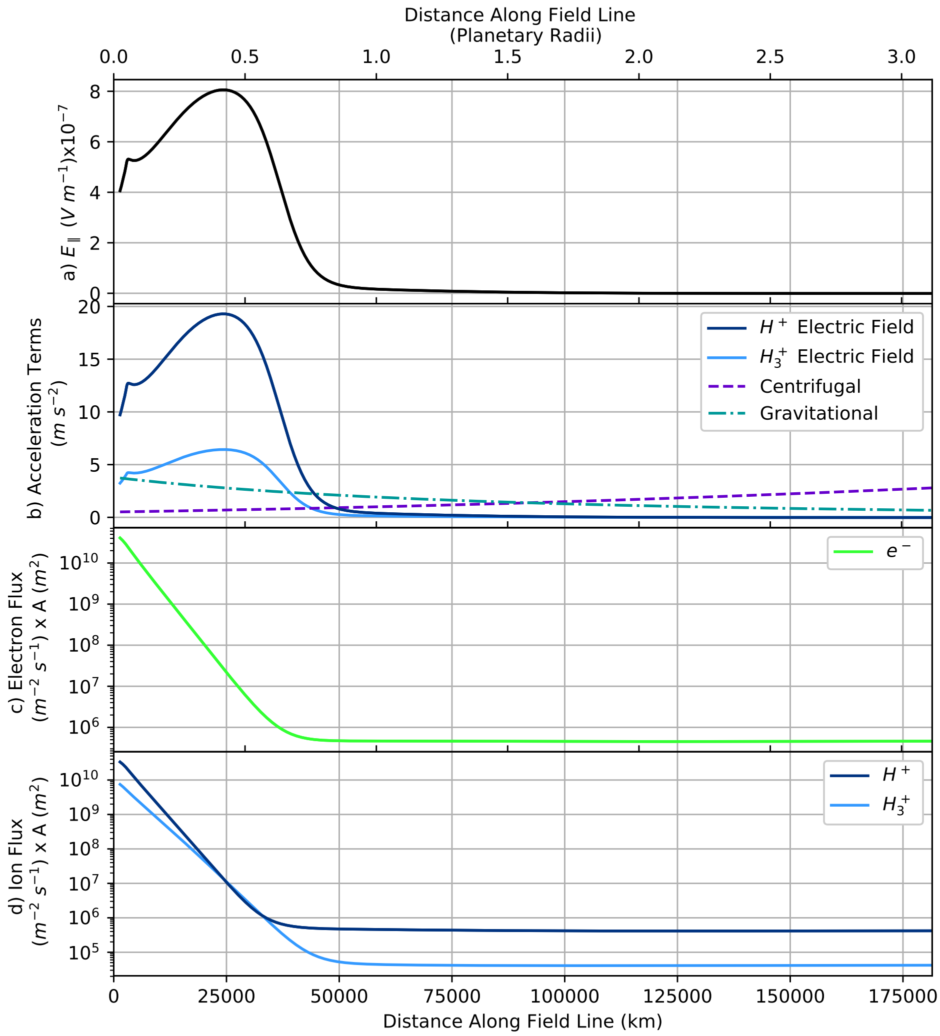

Figure 2. Results for 'run 1' of the ionospheric outflow model where field-aligned currents and centrifugal forces are included, where initial values are T = 700 K, $n_{H^+} = 5 \times 10^{10}\,\mathrm{m}^{-3}$ and $n_{H_3^+} = 2 \times 10^{10}\,\mathrm{m}^{-3}$ for the ionospheric end of the flux tube. a) shows the electric field from 1400 km to 3 R_S in altitude. b) shows the magnitude of the acceleration terms, where solid dark blue is the electric field acting on the H^+ ions, solid pale blue is the electric field acting on the H_3^+ ions, the purple dashed line is the centrifugal acceleration, and the dot-dash teal line is the gravitational acceleration. c) shows the electron flux, scaled to the cross sectional-area and d) shows the ion fluxes scaled to the cross sectional-area, where dark blue is H^+ ions and pale blue is H_3^+ ions.

ature) used are large; we assume that this is the largest source of uncertainty in the model and, therefore, we do not evaluate the intrinsic uncertainties involved with the numerical method used.

Table 1 gives the results of 5 runs used to explore the parameter space in the model. Run 1 and run 2 are described as auroral and terrestrial-like, the results of which are shown in Figures 2 and 3, respectively. Run 3 shows the initial conditions and results for a sub-auroral region with a width of 10° in latitude. This formulation corresponds to an area below the auroral region with no FACs.

The uncertainty in the initial conditions is large, and as such we run the model for each estimation of total particle source for 100 randomly selected initial conditions between the values for 'run 4' and 'run 5' in table 1. These represent the minimum and maximum initial values. When FACs and CF are included, a total particle source rate range of 5.5×10^{27} to $1.3 \times 10^{28}\,\mathrm{s}^{-1}$ is found, corresponding to a total mass source of $5.5 - 17.7\,\mathrm{kg\,s}^{-1}$ (shown as the results for 'run 4' and 'run 5' in table 1). Conversely, the same is done for the exclusion of FACs and CF, where a total particle source rate range of 8.9×10^{26} to $6.8 \times 10^{27}\,\mathrm{s}^{-1}$ is found, corresponding to a total mass source of $0.9 - 6.8\,\mathrm{kg\,s}^{-1}$.

4 Discussion

Field-aligned currents (FACs) and centrifugal forces (CF) enhance ionospheric outflow by increasing the electric field, and hence the acceleration due to the electric field compared to a slowly rotating system in the absence of auroral currents. The electric field (Fig 2a) peaks at around $8\,\mathrm{Vm}^{-1}$ at 25000 km when the CF and FACs are included, but this peak is shown to be lower, $\sim 6.7\,\mathrm{Vm}^{-1}$, when they are excluded. This has a knock on effect with the acceleration due to the electric field (Fig 2b) where when FACs and CF are included the peak is found at $\sim 19\,\mathrm{ms}^{-2}$, but it is found at $\sim 17\,\mathrm{ms}^{-2}$ when excluded.

CFs at Saturn exert a stronger influence over the ionospheric outflow than at Jupiter. Figures 2b and 3b show the acceleration due to gravity (dashed-dotted teal) and CFs (dashed purple). When included, the CF increases and surpasses the magnitude of the gravitational force at around 1.5 planetary radii, thus increasing the number of particles flowing outwards along the field line. Previously, Martin et al. (Submitted), showed that at Jupiter the CF does not surpass the gravitational force until beyond 2 planetary radii owing to the the larger planetary mass. At Jupiter, considering the effects of FACs and CF on ionospheric outflow shows a 90% increase in total mass source rate (from 3.9 to $7.7\,\mathrm{kg\,s}^{-1}$), whereas in this study the inclusion of FACs and CF increase the total mass source from $3.2\,\mathrm{kg\,s}^{-1}$ to $17.7\,\mathrm{kg\,s}^{-1}$, a 450% increase. Thus, CF is relatively more important in driving ionospheric outflow at Saturn than at Jupiter.

Our main finding is that the inclusion of FACs and CF in the ionospheric outflow model increases the output of plasma into the magnetosphere by an order of magnitude. A total particle source rate range of 5.5×10^{27} to $1.3 \times 10^{28}\,\mathrm{s}^{-1}$ is found, corresponding to a total mass source of $5.5–17.7\,\mathrm{kg\,s}^{-1}$ (shown as the results for 'run 4' and 'run 5' in table 1), when FACs and CF are included. Conversely, when FACs and CF are excluded, a total particle source rate range of 8.9×10^{26} to $6.8 \times 10^{27}\,\mathrm{s}^{-1}$ is found, corresponding to a total mass source of $0.9 - 6.8\,\mathrm{kg\,s}^{-1}$.

Felici et al. (2016) presented an event of ionospheric outflow in Saturn's magnetotail, determining a total particle flux of $(6.1 \pm 2.9) \times 10^{27}$ and $(2.9 \pm 1.4) \times 10^{28}\,\mathrm{s}^{-1}$. This particle flux relates to a mass flux of 10 ± 4 and $49 \pm 23\,\mathrm{kg\,s}^{-1}$. The range of values in our study therefore lie within the Felici et al. (2016) range of values, when including CF and FACs. Additionally, previous modeling of Saturn (Glocer et al., 2007) es-

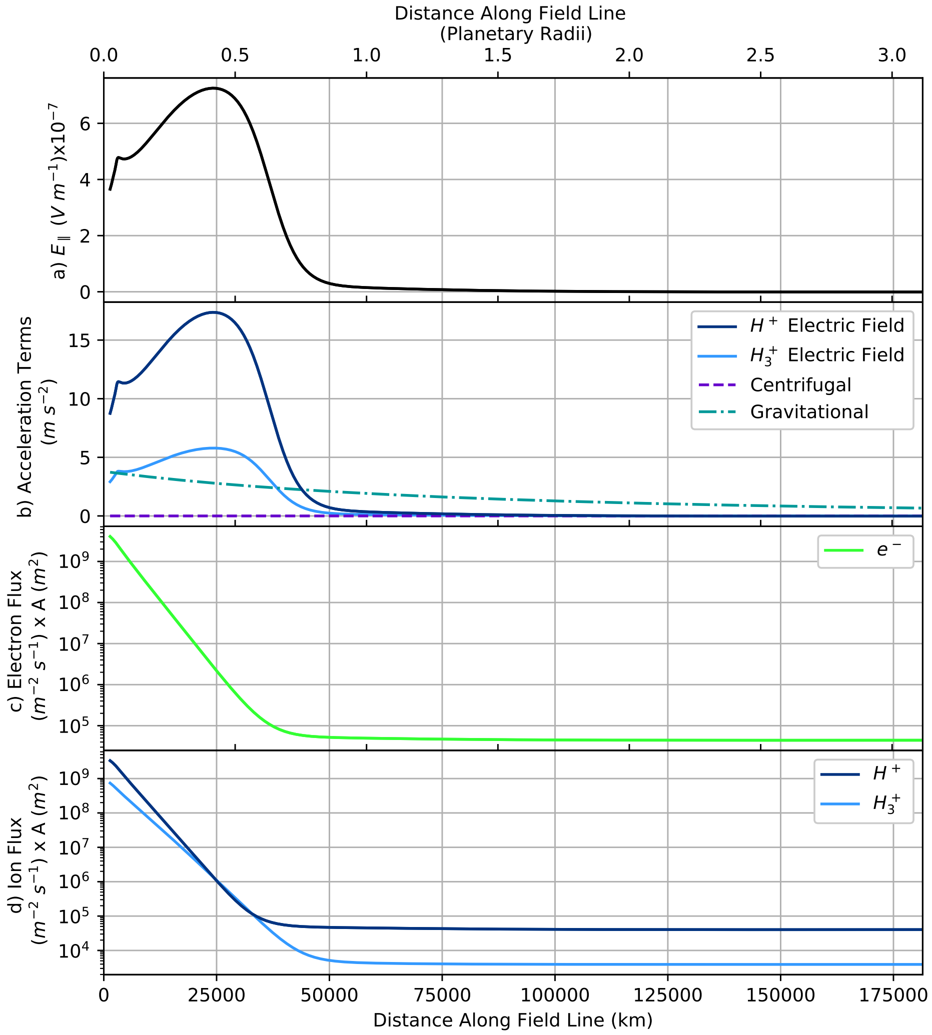

Figure 3. Results for 'run 2' of the ionospheric outflow model where field-aligned currents and centrifugal forces are not included for the same field line as figure 2. Initial values are T = 700 K, $n_{H^+} = 5 \times 10^{10}\,\mathrm{m^{-3}}$ and $n_{H_3^+} = 2 \times 10^{10}\,\mathrm{m^{-3}}$ for the ionospheric end of the flux tube in the same format as Figure 2

timate a total number flux to be 2.1×10^{26} - $7.5\times10^{27}\,\mathrm{s}^{-1}$, which is comparable to the lower values of particle source rate obtained by our model, when excluding CFs and FACs.

As discussed previously, there are other sources of plasma in Saturn's magnetosphere, namely the solar wind and Enceladus. Felici et al. (2016) estimated that the solar wind produces a total particle flux into the magnetosphere of order $10^{27}-10^{28}\,\mathrm{s}^{-1}$, which gives a mass flux of between 10 and $49\,\mathrm{kg\,s^{-1}}$. These values are comparable to the total flux of particles from the ionosphere presented within this study, however, solar wind-sourced particles in Saturn's magnetosphere enter through viscous interactions at the magnetopause (e.g., Delamere & Bagenal, 2010, 2013; Desroche et al., 2013), and as such populate the very outer parts of the magnetosphere. Conversely, plasma from the ionosphere travels along field lines that link to equatorial distances of $< 25\,\mathrm{R_S}$ (Bunce et al., 2008), thus populating the inner and middle magnetosphere of Saturn. It is clear that the introduction of less massive ions to the middle magnetosphere will affect the dynamics of the system as a whole e.g. through modifications to magnetospheric currents and plasma sheet structure through scale height variations.

The middle magnetosphere is populated by other sources and ionic species. Understanding the relative contributions from multiple sources is necessary for interpreting in situ measurements and describing magnetospheric dynamics. Enceladus is situated at $\sim 4\,R_S$ in Saturn's magnetosphere. The moon releases large amounts of water group neutrals which are then ionised. These water group ions are found in the inner and middle magnetosphere of Saturn. Pontius and Hill (2006) and Fleshman et al. (2013) estimate that around 60-100 $\mathrm{kg\,s^{-1}}$ of plasma is sourced from the Enceladus neutrals. Estimating equal amounts of O^+, HO^+, H_2O^+ and H_3O^+ we can surmise that the total particle flux from Enceladus is of the order $\sim 10^{27}\,\mathrm{s}^{-1}$. Thus, the number of particles from the ionosphere is comparable, if not more, than the number of ionised particles from Enceladus, with both sources populating the inner to middle magnetosphere. It is also important to note, that Titan at $\sim20\,R_S$ is also a minor contributor of hydrogen ions in the middle and outer magnetosphere (e.g. Tseng et al., 2011).

Martin et al. (Submitted) argued for the presence of an additional sub-auroral source region powered by radial currents in equatorial region of Jupiter's magnetosphere, based on the data found by Valek et al. (2019). The Juno JADE data showed that the ionospheric sourced plasma was mainly found along field lines that linked to the equator inside of the moon Io and outside of the main auroral oval. At Saturn, this could be occurring on a smaller scale with the radially moving outflow of water ions from Enceladus. We again assume a sub-auroral region of 10° below the original 2° auroral region described above, mapping to the inner and middle magnetosphere of Saturn. Assuming no FACs in the region, but with CF included, the total particle source is found by the model to be 6.1×10^{27} to $1.5\times10^{28}\,\mathrm{s}^{-1}$ which corresponds to a total mass source of $6.7-19.9\,\mathrm{kgs}^{-1}$ for this region alone. Hence, ionospheric outflow may comprise as much as half of the total particle and total mass sources from the entire region of interest.

Another interesting note, is that the FACs in Saturn's auroral regions are heavily modulated by an additional rotating system of FACs which rotate with the planetary period (e.g., Arridge et al., 2011; Provan et al., 2012). The FAC can enhance or depress the outflow of plasma by between 5-10%. With an additional enhancement or depression of FAC of the same magnitude as the fixed local time currents (Hunt et al., 2015), we could see a planetary period modulation of ionospheric outflow of up to 20% at Saturn. A robust study of ionospheric outflow over a range of solar activity and Saturnian season would also be an interesting extension to this work with implications for magnetospheric dynamics.

5 Summary

A model of ionospheric outflow was developed for use at Saturn's auroral regions, including the effects of FACs that are present in these regions. The model utilises the five-moment gyrotropic transport equations, along with an electron energy equation and the assumptions of quasi-neutrality and steady state electron velocity. Using initial conditions appropriate for auroral and sub-auroral conditions, we find a range of total particle and mass source rates of the ionospheric outflow. When including the CFs and FACs, the particle source rate and mass source rate are increased by an order of magnitude compared to previous models and the removal of FACs and CF.

The main results from this study are as follows:

1. The inclusion of the effects of centrifugal force and field-aligned currents in the model increases the expected total particle flux from the ionosphere, which are comparable to values measured in situ by the CAPS instrument on Cassini.
2. We estimate that the total particle source rate arising from ionospheric outflow is between 5.5-13 $\times 10^{27}\,\mathrm{s}^{-1}$, which corresponds to a mass rate of 5.5-17.7 $\mathrm{kg\,s}^{-1}$.
3. An influx of less massive hydrogen-based ions could change the dynamics of the inner and middle magnetosphere of Saturn, where, in previous schools of thought, the area would be water group ion dominated.
4. The increased value of total particle flux is comparable to that of both the solar wind and Enceladus as sources of plasma in the magnetosphere.

Acknowledgments

CJM, LCR and DAC were funded by STFC grant number ST/R000816/1. CTSL was funded by a STFC studentship. CJM acknowledges David Southwood, Sarah Badman and Alex Bader for informative discussion. CJM acknowledges the Europlanet 2020 RI project for funding to attend the Europlanet NA1 workshop: Uniting Planetary Modelling and Data Analysis. The ionospheric outflow model is available on request from CJM and LCR and model outputs are available from a Lancaster University repository with DOI number 10.17635/lancaster/researchdata/315.

References

Arridge, C. S., André, N., Khurana, K., Russell, C., Cowley, S., Provan, G., … others (2011). Periodic motion of Saturn's nightside plasma sheet. *Journal of Geophysical Research: Space Physics*, *116*(A11). doi: 10.1029/2011JA016827

Axford, W. (1968). The polar wind and the terrestrial helium budget. *Journal of Geophysical Research*, *73*(21), 6855–6859. doi: 10.1029/JA073i021p06855

Bagenal, F., & Delamere, P. A. (2011). Flow of mass and energy in the magnetospheres of Jupiter and Saturn. *Journal of Geophysical Research: Space Physics*, *116*(A5). doi: 10.1029/2010JA016294

Banks, P. M., & Kockarts, G. (1973). *Aeronomy.* Academic Press.

Bunce, E., Arridge, C., Cowley, S., & Dougherty, M. (2008). Magnetic field structure of Saturn's dayside magnetosphere and its mapping to the ionosphere: Results from ring current modeling. *Journal of Geophysical Research: Space Physics*, *113*(A2). doi: 10.1029/2007JA012538

Cowley, S., Bunce, E., Stallard, T., & Miller, S. (2003). Jupiter's polar ionospheric flows: Theoretical interpretation. *Geophysical research letters*, *30*(5). doi: 10.1029/2002GL016030

Delamere, P., & Bagenal, F. (2010). Solar wind interaction with Jupiter's magnetosphere. *Journal of Geophysical Research: Space Physics*, *115*(A10). doi: 10.1029/2010JA015347

Delamere, P., & Bagenal, F. (2013). Magnetotail structure of the giant magnetospheres: Implications of the viscous interaction with the solar wind. *Journal of Geophysical Research: Space Physics*, *118*(11), 7045–7053. doi: 10.1002/2013JA019179

Desroche, M., Bagenal, F., Delamere, P., & Erkaev, N. (2013). Conditions at the magnetopause of Saturn and implications for the solar wind interaction. *Journal of Geophysical Research: Space Physics*, *118*(6), 3087–3095. doi: 10.1002/jgra.50294

Dungey, J. W. (1961). Interplanetary magnetic field and the auroral zones. *Physical Review Letters*, *6*(2), 47. doi: 10.1103/PhysRevLett.6.47

Felici, M., Arridge, C. S., Coates, A. J., Badman, S. V., Dougherty, M. K., Jackman, C. M., … Sergis, N. (2016). Cassini observations of ionospheric plasma in Saturn's magnetotail lobes. *Journal of Geophysical Research: Space Physics*, *121*(1), 338–357. doi: 10.1002/2015JA021648

Fleshman, B., Delamere, P., Bagenal, F., & Cassidy, T. (2013). A 1-D model of physical chemistry in Saturn's inner magnetosphere. *Journal of Geophysical Research: Planets*, *118*(8), 1567–1581. doi: 10.1002/jgre.20106

Glocer, A., Gombosi, T., Toth, G., Hansen, K., Ridley, A., & Nagy, A. (2007). Polar wind outflow model: Saturn results. *Journal of Geophysical Research: Space Physics*, *112*(A01304). doi: 10.1029/2006JA011755

Gombosi, T., Cravens, T., & Nagy, A. (1985). A time-dependent theoretical model of the polar wind: Preliminary results. *Geophysical research letters*, *12*(4), 167–170. doi: 10.1029/GL012i004p00167

Hill, T. (1979). Rates of mass, momentum, and energy transfer at the magnetopause. In *Magnetospheric boundary layers* (Vol. 148).

Hill, T., Dessler, A., & Goertz, C. (1983). Magnetospheric models. *Physics of the Jovian magnetosphere*, 353–394.

Hoffman, J. H. (1970). Studies of the composition of the ionosphere with a magnetic deflection mass spectrometer. *International Journal of Mass Spectrometry and Ion Physics*, *4*(4), 315–322. doi: 10.1016/0020-7381(70)85047-1

Hunt, G., Cowley, S., Provan, G., Bunce, E., Alexeev, I., Belenkaya, E., … Coates, A. (2015). Field-aligned currents in Saturn's northern nightside magnetosphere: Evidence for interhemispheric current flow associated with planetary period oscillations. *Journal of Geophysical Research: Space Physics*, *120*(9), 7552–7584. doi: 10.1002/2015JA021454

Jackman, C., Achilleos, N., Bunce, E., Cowley, S., Dougherty, M., Jones, G., … Smith, E. (2004). Interplanetary magnetic field at 9 AU during the declining phase of the solar cycle and its implications for Saturn's magnetospheric dynamics. *Journal of Geophysical Research: Space Physics*, *109*(A11).

Jurac, S., McGrath, M., Johnson, R., Richardson, J., Vasyliunas, V., & Eviatar, A. (2002). Saturn: Search for a missing water source. *Geophysical research letters*, *29*(24), 25–1. doi: 10.1029/2002GL015855

Jurac, S., & Richardson, J. (2005). A self-consistent model of plasma and neutrals at Saturn: Neutral cloud morphology. *Journal of Geophysical Research: Space Physics*, *110*(A9). doi: 10.1029/2004JA010635

Jurac, S., & Richardson, J. (2007). Neutral cloud interaction with Saturn's main rings. *Geophysical research letters*, *34*(8). doi: 10.1029/2007GL029567

Martin, C., Ray, L., DA, C., Lorch, C., Felici, M., & Southwood, D. (Submitted). Evaluating the ionospheric mass source for Jupiters magnetosphere: An ionospheric outflow model for the auroral regions. *Journal of Geophysical Research: Space Physics*, —(-), –. doi: --

Masters, A., Eastwood, J. P., Swisdak, M., Thomsen, M. F., Russell, C. T., Sergis, N., … Krimigis, S. M. (2012). The importance of plasma β conditions for magnetic reconnection at Saturn's magnetopause. *Geophysical Research Letters*, *39*(8). Retrieved from `https://agupubs.onlinelibrary.wiley.com/`

doi/abs/10.1029/2012GL051372 doi: 10.1029/2012GL051372

Moore, L., Galand, M., Mueller-Wodarg, I., Yelle, R., & Mendillo, M. (2008). Plasma temperatures in saturn's ionosphere. *Journal of Geophysical Research: Space Physics*, *113*(A10). doi: 10.1029/2008JA013373

Moses, J. I., & Bass, S. F. (2000). The effects of external material on the chemistry and structure of saturn's ionosphere. *Journal of Geophysical Research: Planets*, *105*(E3), 7013–7052. doi: 10.1029/1999JE001172

Pontius, D. (1995). Implications of variable mass loading in the Io torus: The Jovian flywheel. *Journal of Geophysical Research: Space Physics*, *100*(A10), 19531–19539. doi: 10.1029/95JA01554

Pontius, D., & Hill, T. (1982). Departure from corotation of the Io plasma torus: Local plasma production. *Geophysical Research Letters*, *9*(12), 1321–1324. doi: 10.1029/GL009i012p01321

Pontius, D., & Hill, T. (2006). Enceladus: A significant plasma source for Saturn's magnetosphere. *Journal of Geophysical Research: Space Physics*, *111*(A9). doi: 10.1029/2006JA011674

Provan, G., Andrews, D. J., Arridge, C. S., Coates, A. J., Cowley, S., Cox, G., ... Jackman, C. (2012). Dual periodicities in planetary-period magnetic field oscillations in Saturn's tail. *Journal of Geophysical Research: Space Physics*, *117*(A1). doi: 10.1029/2011JA017104

Ray, L., Galand, M., Delamere, P., & Fleshman, B. (2013). Current-voltage relation for the Saturnian system. *Journal of Geophysical Research: Space Physics*, *118*(6), 3214–3222. doi: 10.1002/jgra.50330

Schunk, R., & Nagy, A. (2000). Ionospheres. *Plasma Physics, and Chemistry, Cambrige University Press*.

Southwood, D., & Kivelson, M. (2001). A new perspective concerning the influence of the solar wind on the Jovian magnetosphere. *Journal of Geophysical Research: Space Physics*, *106*(A4), 6123–6130. doi: 10.1029/2000JA000236

Tseng, W.-L., Johnson, R. E., Thomsen, M. F., Cassidy, T. A., & Elrod, M. K. (2011). Neutral h2 and h2+ ions in the saturnian magnetosphere. *Journal of Geophysical Research: Space Physics*, *116*(A3). doi: 10.1029/2010JA016145

Valek, P., Allegrini, F., Bagenal, F., Bolton, S., Connerney, J., Ebert, R., ... Wilson, R. (2019). Jovian High-Latitude Ionospheric Ions: Juno In Situ Observations. *Geophysical Research Letters*, *46*. doi: 10.1029/2019GL084146

Vasyliūnas, V. (2008). Comparing Jupiter and Saturn: Dimensionless input rates from plasma sources within the magnetosphere. *Ann. Geophys.*, *26*(6), 1341–1343. doi: angeo-26-1341-2008

Yamauchi, M. (2019). Terrestrial ion escape and relevant circulation in space. *Annales Geophysicae*, *37*(6), 1197–1222. Retrieved from https://www.ann-geophys.net/37/1197/2019/ doi: 10.5194/angeo-37-1197-2019

Yau, A. W., Abe, T., & Peterson, W. (2007). The polar wind: Recent observations. *Journal of Atmospheric and Solar-Terrestrial Physics*, *69*(16), 1936–1983. doi: 10.1016/j.jastp.2007.08.010